

A numerical approach for simulating the behaviour of timber shear walls

Wei Yuen Loo*, Pierre Quenneville^a and Nawawi Chouw^b

*Department of Civil and Environmental Engineering, School of Engineering,
University of Auckland, New Zealand*

(Received August 28, 2011, Revised February 6, 2012, Accepted April 2, 2012)

Abstract. A numerical approach to simulate the behaviour of timber shear walls under both static and dynamic loading is proposed. Because the behaviour of timber shear walls hinges on the behaviour of the nail connections, the force-displacement behaviour of sheathing-to-framing nail connections are first determined and then used to define the hysteretic properties of finite elements representing these connections. The model nails are subsequently implemented into model walls. The model walls are verified using experimental results for both monotonic and cyclic loading. It is demonstrated that the complex hysteretic behaviour of timber shear walls can be reasonably represented using model shear walls in which nonlinear material failure is concentrated only at the sheathing-to-framing nail connections.

Keywords: timber shear walls; midply; numerical simulation; hysteresis; nail connections; cyclic; monotonic

1. Introduction

1.1 Background

Timber shear walls are widely used to provide lateral force resistance for buildings of timber-framed construction. Timber shear walls demonstrate an ability to behave in a highly ductile manner, and are efficient dissipaters of energy during dynamic loading. Wood structures incorporating these walls have thus performed well during actual earthquake events. The inherent ductility of these structures allows significant deformation to take place, but mostly without catastrophic collapse.

Because timber shear walls are widely used in timber construction and are frequently designed to withstand earthquake induced forces, there has in recent years been a significant amount of research gone into simulating both the behaviour of timber shear walls, and the building structures which incorporate them.

This paper presents a new approach to simulate the behaviour of timber shear walls, with careful

*Corresponding author, Ph.D. Candidate, E-mail: wloo002@aucklanduni.ac.nz

^aProfessor, E-mail: p.quenneville@aucklanduni.ac.nz

^bAssociate Professor, E-mail: n.chouw@aucklanduni.ac.nz

consideration given to different framing, sheathing, and nail connection configurations, during the modelling process. The model walls can be quickly constructed and tested under monotonic, cyclic, and dynamic loading. A discussion of previous research, and the advantages of the proposed method is presented in the following two sections.

1.2 Previous research

An overview of some research on the modelling of timber shear walls in recent years is presented below.

Ayoub (2007) proposed a model for the nonlinear seismic analysis of wood building structures. Shear walls were modelled with sheathing panels connected to framing members using distributed interface elements to model the nails. The shear behaviour of the nails in two perpendicular defined directions were uncoupled. Ayoub gave particular emphasis to strength and stiffness degradation observed in the hysteretic behaviour of the nail connections, and obtained good agreement between the response of his model wall, which incorporated these connections, and the response of comparable experimental shear walls under shake table loading.

Judd and Fonseca (2005) proposed a model wall using an oriented pair of coupled nonlinear springs for the nail connections. The initial orientation of the slip of each nail connection was used to set the orientation of the nail slip for the entirety of loading. This was based on the observed tendency of nails to move along a single orientation during excitation. The model is capable of both monotonic and cyclic analysis, however some programming effort is required to implement the spring pair representing the nails. The finite element response and measured experimental result showed close alignment with each other.

Blasseti *et al.* (2008) presented a simplified methodology for modelling wood shear wall behaviour. A combination of basic elements available in most finite element packages, were used to represent the nail connections. This obviated the need for extensive programming. The nail connection hysteretic model, while having the limitation of an indefinite increase of strength with displacement, nevertheless replicated pinching behaviour well, and when implemented in the wood shear wall model, produced excellent results with the behaviour of the numerical walls closely aligning with those of comparable experimental walls in terms of observed hysteretic behaviour and overall energy dissipation.

Xu and Dolan (2009a) improved on a general hysteretic model, Bouc-Wen-Barer-Wen, to produce a nail connection model that is nonlinear, history dependent, and includes stiffness and strength degradation and pinching. The hysteresis model was embedded in commercially available software, as a user-defined element which accounted for the coupling property of the nail joint action. A detailed shear wall was modelled and analysed, with the numerical results agreeing well with experimental test data. Xu and Dolan (2009b), also proposed a macro-shear wall model which represented the hysteretic behaviour of a whole shear wall when subjected to lateral loads, without the need for individual nail connections.

1.3 Proposed method

The proposed modelling methodology utilises a well-known and well-established exponential relationship to describe nail load-slip behaviour. The parameters of this curve are based on experimental data obtained from a large suite of tests, both cyclic and monotonic, from various

researchers. These parameters are used to define a benchmark curve which is raised or lowered to match different values of lateral ultimate connection strength, F_{ult} , while the ultimate displacement, δ_{ult} , is assumed to remain unvaried for all sizes and strengths of nail connections. The ultimate strengths of nail connections obtained using a mechanics based analytical method are compared with the values obtained from experiments on actual nail connections, and a mathematical relationship found which can be used to predict the ultimate connection strength F_{ult} for various configurations of shear walls, taking into account differences in nail, sheathing and framing properties.

A simple hysteretic model is proposed which includes for pinching effects as well as strength and stiffness degradation with increasing displacement. While the nail model perhaps lacks the accuracy of some of the aforementioned models proposed by other researchers, it has the advantage of no programming being required to define the hysteretic behaviour. The only work required is to enter the coordinates of the force-displacement envelope curve, and the setting of two simple parameters to define the degree of ‘pinching’ of the hysteresis loops. Double shear connections are accounted for as well as single shear connections.

The behaviour of model numerical shear walls which implement these model nails, align well with experimentally tested walls placed under both monotonic and cyclic loading schedules. The advantages of the method include (1) its simplicity, (2) the use of a simple hysteresis model which can be implemented quickly in a single finite element in SAP2000 without any programming required, (3) the nail model, in spite of its simplicity, nevertheless capturing well the pinching and degrading effects of actual nails, (4) a new quick method to determine the envelope curves for both monotonic and cyclic behaviour of nail connections, for shear wall of different configurations and material properties, and (5) the ability to observe both global behaviour of a model shear wall and the behaviour of individual nail connections, throughout a monotonic or cyclic loading process.

Numerical modelling results for two types of shear walls, standard and midply, are presented in this paper. Standard shear walls generally consist of one ply of structural sheathing, nailed directly to a single layer of timber framing (see Figs. 1(a), (b)). With midply walls, structural sheathing is placed and secured in between two layers of timber framing (see Fig. 1(c)).

When a shear wall with hold-down connectors comes under horizontal loading, it behaves as if it were a vertically oriented cantilever, rigidly secured to the base. The studs at each end of the shear

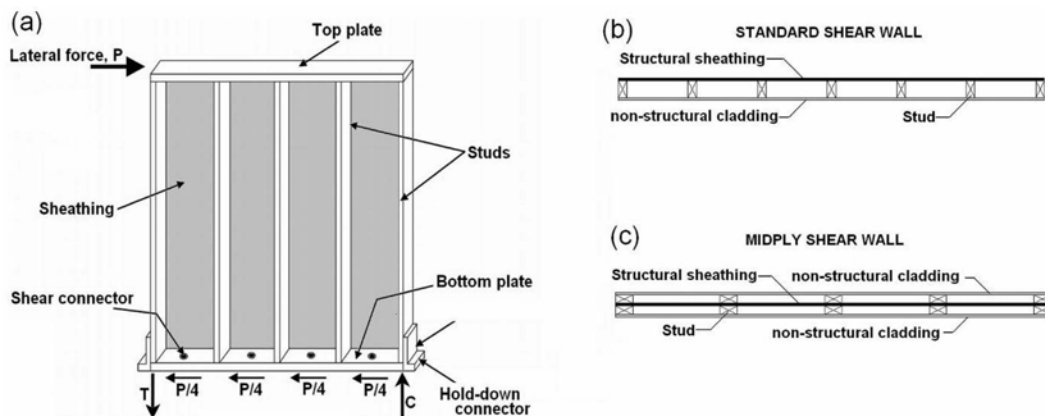


Fig. 1 Timber shear walls (a) how shear walls resist lateral force (b) standard configuration and (c) midply configurations

wall, one in tension, the other in compression, resist the bending moment induced by lateral loading. The purpose of the sheathing is to prevent shear (racking) deformations to the wall. The ductile behaviour of timber shear walls relates not to the timber material itself (which is typically brittle), but the connections attaching sheathing to framing (Buchanan 2007).

Because of the aforementioned influence of the nail connections on overall shear wall behaviour, Section 2 discusses in some detail how these connections are modelled. The remaining parts of the paper deals with the overall behaviour of model walls incorporating the model nails, and the verification of the proposed approach using experimental results obtained by other researchers.

2. Nail connections

Based on hysteresis parameters obtained from experimental testing, a force-displacement curve for nail connections is constructed. This curve takes the form of the Foschi exponential curve (Dolan and Madsen 1992). It acts as a ‘benchmark’ that can be readily adjusted to agree with the ultimate strength, F_{ult} , of any particular nail connection.

To determine the ultimate strength of a nail connection, an initial value is first arrived at by using the European yield model (EYM) equations provided by the American Forest and Paper Association (1999). This value is then increased to take into account factors ignored by EYM theory. These factors are end-fixity of nails, inter-member friction, and string resistance. The benchmark curve is then adjusted to agree with this finalised value of F_{ult} .

Nail connections with force-displacement curves so determined are numerical modelled using the finite element software SAP2000 (Computers and Structures, Inc. 2009).

2.1 Benchmark envelope curve

The benchmark force-displacement relationship for modelling nails, will take the form of the well-known Foschi exponential curve (Dolan and Madsen 1992). Eq. (1) describes the curve between zero and ultimate displacement, δ_{ult}

$$Force = (F_0 + K_1 \delta) \cdot [1 - \exp(-K_0 \delta / F_0)] \quad (1)$$

and Eq. (2) describes the relationship for displacements beyond δ_{ult}

$$Force = K_2 \delta + (F_{ult} - K_2 \delta_{ult}) \quad (2)$$

The parameters F_0 , F_{ult} , δ_{ult} , K_0 , K_1 , and K_2 (Fig. 2), are all empirically obtained. In addition to the Foschi curve parameters, the ‘pinching’ strength F_1 is also indicated. Pinching takes place as a result of loss of strength and stiffness in the wood material during cyclic loading (Buchanan 2007).

Dolan and Madsen (1992), reported on a series of monotonic and cyclic tests carried out on nail connections. These were carried out on nails connecting plywood to framing lumber, and nails connecting wafer-board to framing lumber. Only the results pertaining to plywood will be considered in this section. Three types of numerical simulations were carried out. Monotonic (one-directional) with a displacement rate of 10 mm/min, slow cyclic testing with a displacement rate of 10 mm/min, and rapid cyclic testing with a displacement rate of 300 mm/min.

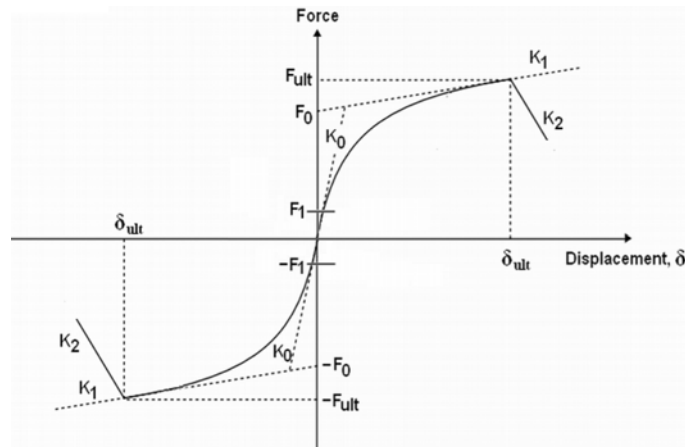


Fig. 2 Foschi envelope curve parameters

Dolan and Madsen found that the angle between direction of loading and grain orientation (whether of sheathing or framing), had little effect on the force-displacement relationship. They also found that results from slow cyclic loading were practically indistinguishable from those obtained by fast cyclic loading. Furthermore, the hysteresis loops produced by nail connections under cyclic loading, were found to be bounded by the monotonic force-displacement envelopes obtained for nail connections of the same configuration. This has important implications for the modelling of nail connections. For a particular nail connection, the same force-displacement envelope can therefore be used for both monotonic and cyclic loading conditions.

The averaged values of the Foschi exponential curve parameters obtained by Dolan and Madsen are shown in Table 1.

Note that for the parameter K_1 , which describes stiffness after yielding of the connection, there was variation related to the orientation of the nail against the grain orientations of both the sheathing and framing. However Dolan and Madsen found that these variations would not

Table 1 Averaged Foschi parameter values according to Dolan and Madsen (1992)¹

Foschi parameter	Parameter value ²
F_0 (N)	920
F_1 (N)	193
K_0 (N/mm)	1182
K_1 (N/mm)	50
K_2 (N/mm)	-42
δ_{ult} (mm)	9
F_{ult} ³ (N)	1370

¹Nails were flat headed, hot dipped galvanised, 64 mm in length, 3.33 mm diameter. Sheathing was of 9 mm Canadian softwood ply and framing was of 38 × 89 mm spruce-pine-fir (SPF).

²Average over all tests - monotonic, slow cyclic, and rapid cyclic

³ F_{ult} calculated from Eq. (1), for $\delta = \delta_{ult} = 9$ mm.

significantly alter the overall characteristics of the force-displacement curves when used in the modelling of shear walls.

The values of Table 1 are input to Eqs. (1) and (2), and a benchmark force-displacement curve is created, which applies specifically to the nail connections tested by Dolan and Madsen. The benchmark force-displacement curve can be applied to nail connections of various configurations, with adjustment to the curve made for any particular ultimate strength, F_{ult} .

F_{ult} for nail connections is found in accordance with the method discussed in Section 2.2. Once F_{ult} is found, the specific force-displacement curve of a nail connection is established by simply multiplying the ordinate values of the points on the Dolan-Madsen benchmark curve by $F_{ult}/1370$ N. This will naturally result in the stiffness values, K_0 , K_1 , and K_2 also being adjusted by $F_{ult}/1370$ N (note that 1370 N is the F_{ult} obtained by Dolan and Madsen; see Table 1).

Only the force values of the points on the benchmark curve, are adjusted - not the displacement values. This is because small diameter dowel connections, such as nails and screws, have been found to have similar F/F_{ult} - displacement curves (Thelandersson and Larsen 2003). Thus screws and nails of various diameters will attain their respective ultimate strengths at a similar level of displacement. This enables them to be used and to act together in a joint. Thelandersson and Larsen (2003) proposed an ultimate displacement of 8 mm for nail connections, while Dolan and Madsen's tests obtained averages of 9 mm for both plywood and waferboard sheathing. The US Department of Agriculture proposes a typical ultimate displacement slightly exceeding 9 mm (U.S. Dept. of Agriculture 2010). For these reasons it has been decided to adopt 9 mm as the ultimate displacement for the nail connections modelled in this paper.

2.2 Determination of nail ultimate strength

The European yield model (EYM) theory provides a mechanics based approach to determine the strength of dowel connections under lateral loading. Dowel connections under both single-shear, and double-shear are considered. EYM theory assumes four basic modes of failure for dowel connections. The mode of failure mainly relates to whether failure will first occur from crushing of the wood fibres by a relatively rigid dowel, or instead from plastic hinging developing in the dowel connector. For nail connections, failure of the connection relates more to inelastic distortion of the nails - rather than the crushing of the wood fibres. Detailed descriptions of these various failure modes are provided by Aghayere and Vigil (2007).

When calculating the ultimate lateral strength of a nail connection, the EYM formulas take into account, dowel bearing strength, $F_{e,ult}$, dowel bending strength, $F_{b,ult}$, nail diameter, sheathing thickness, and nail penetration. There are various versions of the EYM formulas in use. The formulas used in this research are those adopted by the American Forest and Paper Association (1999).

The dowel bearing strength, $F_{e,ult}$, deserves further mention, as the strength and behaviour of nail connections is largely determined by this property. The dowel bearing strength provides the resistance to the movement of a laterally loaded nail through the connected wood material. It is a function of the specific gravity of the wood, SG , and the nail diameter, D . The relationship is described by Eq. (3) (note that D is in metres).

$$F_{e,ult} = 43333504 \times SG^{1.07} / D^{0.17} \quad (3)$$

Table 2 Dowel bearing strengths, $F_{e,ult}$, for various types of wood

Wood material	Specific gravity, SG	$F_{e,ult}$ (MPa) ¹
Canadian Softwood Ply	0.45 ⁽²⁾	49
Oriented Strand Board & waferboard	0.64 ⁽³⁾	72
Douglas fir larch	0.49 ⁽⁴⁾	54
Hem fir	0.46 ⁽⁴⁾	51
Spruce-Pine-Fir (SPF)	0.42 ⁽⁴⁾	46

¹Calculated from Eq. (3), for 3.05 mm diameter nails.

²From CertiWood (2004).

³From Structural Board Association (2004).

⁴Canadian Wood Council (2009).

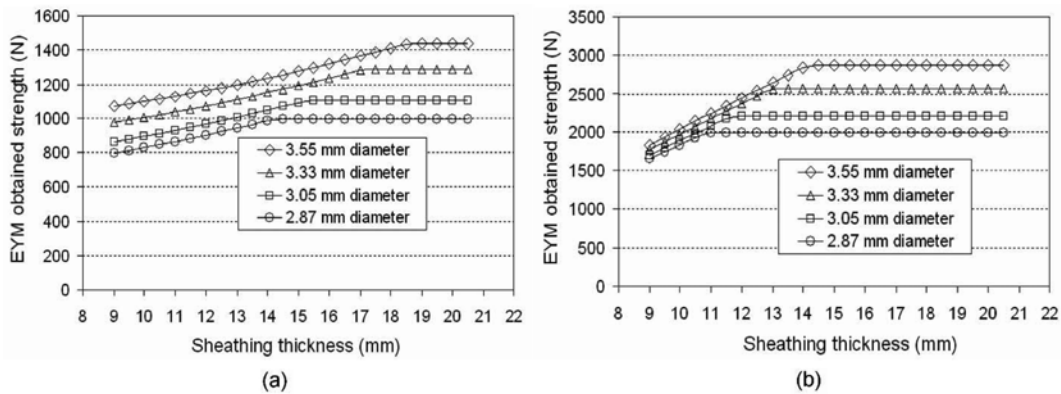


Fig. 3 EYM lateral strengths for OSB sheathing to SPF framing. Nails in (a) single-shear and (b) double shear

The value obtained for $F_{e,ult}$ is input to the EYM equations to find the connection strengths for each of the various yield modes. There are various versions of these EYM equations. The equations adopted in this paper are those provided by the American Forest and Paper Association (1999).

Table 2 shows values of dowel bearing strengths calculated for various framing and sheathing materials (for 3.05 mm diameter nails). Note that for nail connections, $F_{e,ult}$ is independent of the angle between the direction of loading and the direction of the grain (this is not the case for larger diameter fasteners such as bolts).

The ultimate strengths, which are the minimum calculated values out of all the possible modes of failure, are obtained and plotted for various sheathing thicknesses. A minimum nail penetration into the framing timber of 10 nail diameters (10D) is assumed (American Forest and Paper Association 1999). Figs. 3(a) and (b) shows these relationships for single-shear and double-shear connections, respectively. Relationships are provided for 2.87, 3.05, 3.33, and 3.55 mm nails attaching OSB (oriented strand board) sheathing (SG = 0.64) to SPF (spruce-pine- fir) framing (SG = 0.42).

In Fig. 3(a) the sloping portion of the relationships relates to mode III_s behaviour, whereas the flat parts are associated with mode IV behaviour. Mode III_s behaviour involves the forming of a single plastic hinge within the main member (the timber framing), while the length of fastener within the

side member (the sheathing) remains relatively un-deformed thus causing the sheathing to experience significant crushing of wood material. However with increasing thickness of sheathing, the critical failure mode shifts into mode IV, where two plastic hinges form, one within the sheathing and one within the framing. (Aghayere and Vigil 2007).

The flat, horizontal portion of the relationships of Fig. 3(b) (double shear) relates to mode IV failure, in which three plastic hinges form in the nail - one hinge in each of the two outside members and one hinge in the middle member. The sloping part of the relationships, are associated with the brittle I_m failure mode. Mode I_m involves crushing of the sheathing material by a rigid, un-deformed nail (Aghayere and Vigil 2007).

However for experimental testing of midply walls, in which nails connections are under double shear, Varoglu *et al.* (2006) did not report of any brittle damage to the sheathing of midply walls that would have indicated Mode I_m failure. Furthermore, under cyclic loading, midply walls demonstrate high levels of ductility and are efficient dissipaters of energy. Both of these characteristics are consistent with a mode IV connection failure, but not mode I_m failure. Therefore, for the modelling of double-shear nail connections in midply walls, the ultimate strengths associated with mode IV failure will be used in all considered cases – even for those cases in which EYM theory would suggest mode I_m failure.

Experimentally obtained ultimate strength values for various single-shear nail connections, are averaged and shown in Table 3, along with the theoretical EYM calculated values.

The theoretical EYM lateral strengths of various single-shear nail connections are plotted against their corresponding experimentally obtained values in Fig. 4.

Table 3 Nail strengths: Averaged experimental, and theoretical (EYM)

Sheathing ¹ & thickness (mm)	Framing ¹	Nail type	Nail ² length (mm)	Nail diameter (mm)	Ultimate strength, F_{ult}		Reference
					Experiment (N)	EYM (N)	
OSB, 11.1	Hem fir	6d *	51	2.9	1239	889	Coyne (2007)
OSB, 11.1	Hem fir	8d *	64	3.3	1435	1066	"
OSB, 11.1	Hem fir	10d *	76	3.8	1581	1203	"
OSB, 15.9	Hem fir	10d *	76	3.8	1587	1395	"
OSB, 19.1	Hem fir	10d *	76	3.8	1755	1544	"
CSP, 9	SPF	8d *	64	3.3	1370	917	Dolan and Madsen (1992)
Waferboard, 9	SPF	8d *	64	3.3	1325	974	"
OSB, 11.1	Hem fir	8d *	64	3.3	1441	1066	Ekiert and Hong (2006)
OSB, 11.1	Doug.fir-larch	8d +	60	2.9	1226	900	Fonseca and Rabe (2009)
CSP, 11.9	Doug.fir-larch	8d +	60	2.9	1014	760	Fonseca <i>et al.</i> (2006)
CSP, 11.9	Doug.fir-larch	8d +	64	3.3	1076	930	"

¹Refer to Table 2 for specific gravities of wood material when calculating EYM ultimate strength

²For nail penetration, subtract sheathing thickness from nail length. Note that all nails exceed standard penetration of 10D.

*common nails

+cooler nails

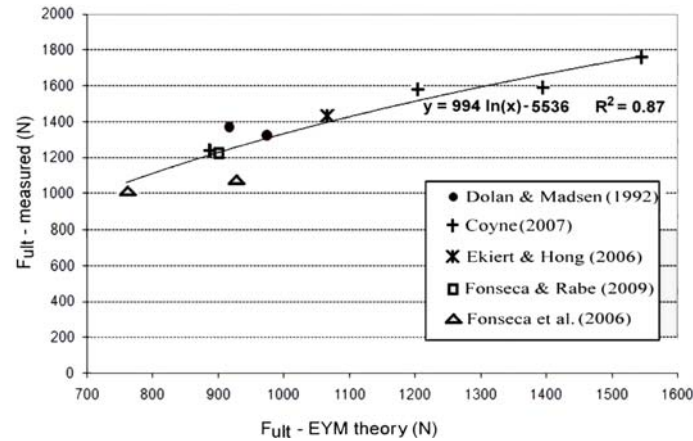


Fig. 4 Relationship between experimentally measured values for ultimate nail strength, and values obtained from EYM theory (single-shear connections)

Based on a least squares fit, a logarithmic curve was preferred over a straight line, with the coefficient of determination, R^2 , for the logarithmic curve being 0.87 and that for a straight line fit being 0.83. The chosen logarithmic relationship is described by (Eq. (4))

$$F_{ult} = 994 \ln(F_{ult(EYM)}) - 5536 \quad (4)$$

From Fig. 4, it can be seen that EYM theory generally underestimates the experimentally measured lateral strength. The reasons for this likely relate to the way in which the EYM equations conservatively ignore the following: (1) the end fixity of the dowel, (2) the inter-member friction between sheathing and framing, and (3) the ‘string’ resistance which develops from nail tension (Smith *et al.* 2001), (American Forest and Paper Association 1999). A brief description of each of these effects follows.

The end fixity effect arises from resistance to rotation at the end(s) of the dowel fasteners. For fasteners in general, end fixity is influenced by the fastener head size, the lateral load level, the size of any washers where they may exist, and the amount of dimensional change in the connected members during loading (American Forest and Paper Association 1999). The effects of end fixity can be quite significant. For example, the New Zealand structural timber code recognises this by allowing a 40% increase in strength, where flathead nails are used with plywood or particle board (NZS3603 1993).

Friction between connected timber members is not accounted for in the EYM equations. This is because of difficulties in predicting the actual amount of frictional force, and also because of the fact that friction would be expected to diminish as the wood shrinks or the connection relaxes (American Forest and Paper Association 1999). However, in spite of all this, inter-member friction can contribute in a significant way to the actual load capacity of nail connections (Smith *et al.* 2001).

Normally the shear resistance over the cross-section of the nail provides the lateral resistance of a nailed connection. However when displacement of a deeply penetrating nail connection becomes significantly large, at least part of the nail shank becomes deformed and bends to align closely with the orientation of the applied lateral load on the connection. When this happens, a part of the nail’s

tension strength will contribute to the lateral resistance already provided by the shear resistance of the nail shank. This so called ‘string’ resistance is ignored in the EYM equations.

The respective contributions to connection strength, of end fixity, inter-member friction, and string resistance, are difficult to accurately quantify. However, it is reasonable to expect that the EYM equations, in ignoring these three factors, will produce conservative values for ultimate lateral strength. While a conservative approach is appropriate for design, it is not appropriate for the modelling of actual nail connection behaviour. Therefore, the ultimate lateral strength, F_{ult} , for modelling is obtained from Eq. (4).

For actual nails in double-shear (the case for midply walls), obtaining experimentally confirmed values for ultimate strength is problematic. This is because midply walls are a recently developed concept, and hence little is found in the literature relating to nail connection tests, in which thin sheathing material is secured between two framing members. Therefore, in order to derive actual lateral strengths from theoretical EYM values, the procedure adopted for single-shear connections is extended to double shear connections.

However, unlike the case for nails in single-shear, for double-shear connections, end-fixity will not contribute to the assumed difference that exists between theoretical and actual lateral strengths. This is because only mode IV failure is assumed for midply wall nail connections in double shear, as previously discussed. However, for connections in double shear, only mode III_s behaviour is influenced by end-fixity (American Forest and Paper Association 1999).

Thus, for double-shear nail connections, only inter-member friction and string resistance, but not end fixity, will be considered when adjusting the theoretical EYM strengths up to their respective actual strengths. This means that for a single shear plane of a double-shear nail connection, the discrepancy between the theoretical EYM strengths and actual strengths will be assumed to be only two-thirds that which would apply for the case of an equivalent nail connection in single shear. Thus the strength of a double shear connection is found as follows

$$F_{ult} = F_{ult(EYM)} + \frac{2}{3}(F_{uef} - F_{ult(EYM)}) \quad (5)$$

where F_{uef} is the ultimate strength which would have been the case if end-fixity effects did contribute, and $F_{ult(EYM)}$ is the theoretical ultimate strength for double shear. F_{uef} is a function of $F_{ult(EYM)}$, and is found by applying Eq. (4) to half the theoretical connection strength, and then doubling this value

$$F_{uef} = 2 \times (994 \ln(0.5 F_{ult(EYM)} - 5536)) \quad (6)$$

The relationship of Eq. (6) is substituted for F_{uef} in Eq. (5), and after re-arranging, the ultimate connection strength, F_{ult} , for a double shear connection can be expressed in terms of the theoretical value $F_{ult(EYM)}$ as follows

$$F_{ult} = \frac{F_{ult(EYM)} + 3976 \ln(0.5 F_{ult(EYM)}) - 22144}{3} \quad (7)$$

Note that values for F_{ult} and $F_{ult(EYM)}$ include for the strength of both shear planes in a double-shear connection.

It should be emphasised that adopting the ‘two-thirds’ rule relies on the assumption that for an equivalent single-shear connection, the effects of inter-member friction, string resistance, and end-

fixity would have contributed equally to the difference between the theoretical EYM connection strength and the actual connection strength. While this assumption requires confirmation of its validity, for the purposes of modelling double shear nail behaviour in this paper, it will be adopted, with the understanding that Eqs. (5) to (7) could see modification in the light of future research.

2.3 Nail connections model

Links capable of modelling nonlinear force displacement behaviour are used to represent the sheathing-to-framing nailed connections. The multi-linear plastic link of SAP2000 allows the definition of a nonlinear load-slip curve in two mutually perpendicular directions. The strength and stiffness degradation can be modelled with this link, and the hysteretic behaviour replicated.

Multi-linear plastic link elements are used to connect two nodes (joints). One link element consists of six springs (see Fig. 5(a)). Three springs relate to translations U_1 , U_2 , and U_3 , and three springs relate to rotations R_1 , R_2 , and R_3 . Note that in this nail model, the stiffness of the longitudinal spring (in the U_1 direction) and the values of stiffness for the three rotational springs are set to zero.

The multi-linear plastic element allows the input of force-displacement relationships (for translational degrees of freedom), and moment-rotation relationships (for rotational degrees of freedom). Separate parameters are available to define the way strength and stiffness can change with loading history. The element can thus be used to describe the hysteretic behaviour of nail connections.

For modelling the nail connections, only the U_2 and U_3 directions (both of which relate to shear) are considered. The same load-displacement relationship is input for both directions. Dolan and Madsen (1992) found the force-displacement behaviour of nails connecting sheathing to framing to be largely directionally independent. The force-displacement behaviour along the U_2 and U_3 directions are assumed to be independent of each other.

It should be noted here that Ayoub (2007), also proposed a connection model which assumed independence between shear behaviour along, and perpendicular to the grain, and Blasseti *et al* (2008) used two springs to represent shear behaviour along the grain, and two springs for across the grain, for a total of four springs per connection. Behaviour along the grain was uncoupled from

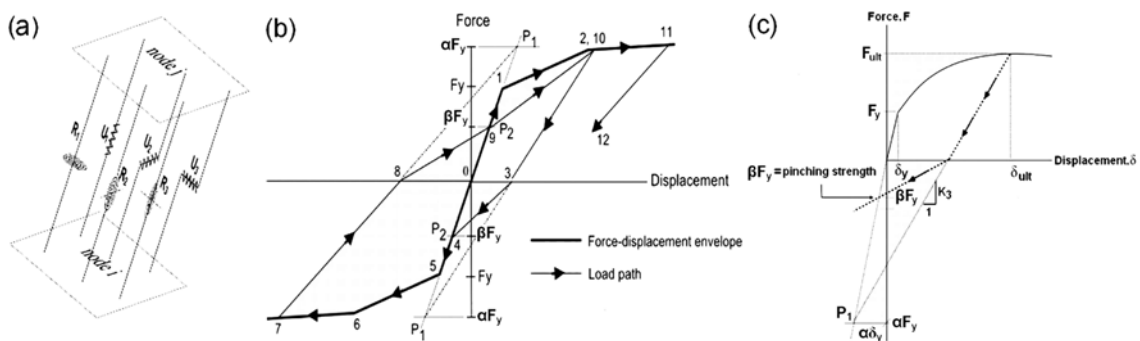


Fig. 5 Nail connection (a) multilinear plastic link element adopted consists of translational and rotational springs (b) multi-linear plastic link –‘pivot’ hysteresis type, and (c) determination of hysteresis parameters α , and β

behaviour perpendicular to the grain. As mentioned in Section 1.2, Ayoub (2007) and Blasseti *et al.* (2008) both obtained good alignment with experimental results when their proposed connections were implemented in model shear walls.

Judd and Fonseca (2005) proposed the use of an oriented pair of nonlinear springs. Their model takes into account the fact that connection stiffness and strength change not only relative to the amount of movement of the nail connection, but also displacement trajectory during cyclic loading. Judd and Fonseca proposed an analytical model in which a spring pair was oriented along the initial displacement orientation of the nail connection. This was done because it is argued that the tearing of the sheathing during loading of the wall limits the movement of the nail inside a relatively narrow channel. It was found that there was a performance improvement in predicting the response of a model wall, over using a non-oriented, uncoupled spring pair. For predicting ultimate displacement, the increased accuracy of the non-oriented spring pair over the uncoupled oriented spring pair was 3% closer to the actual, for ultimate strength 12.8% closer to the actual, and for energy dissipation 10.8% closer to the actual.

Vessby *et al.* (2010), considered four different spring pair models; one uncoupled, and three different types of coupled. Vessby *et al.* found that while a coupled spring pair model was preferable to an uncoupled model, the uncoupled models would require calibration against experimental tests on nails performed for directions other than parallel and perpendicular to the grain of wood.

Considering all of the above, it was decided that to keep the analysis relatively simple with a minimum need of programming effort required, the uncoupled spring pair model would be adopted for the modelling of the nail connections. The possibility of a small over-prediction of strength should be borne in mind when carrying out the analysis, but this is offset by the convenience of choosing the uncoupled spring pair model.

A pivot hysteresis model was adopted to model the force-displacement behaviour of the nail connections. This hysteresis model allows for degradation of stiffness and strength under repeated loading, thereby allowing the pinching effect typical of nail connections to be replicated. It directs both unloading and reloading towards pre-defined pivot points. The way in which pivot points are used to control hysteretic behaviour is shown in Fig. 5(b).

The P_1 pivot points are located at the intersection of the projected line of the first linear portion of the force-displacement relationship, and the horizontal line through αF_y . For unloading between a point on the force-displacement curve, and zero force, the force-displacement line is directed towards P_1 on the opposite side of the displacement axis. The unloading path is redirected towards the pivot point P_2 when it crosses the x -axis. P_2 is located at the intersection of a horizontal line through βF_y , and the elastic portion of the force-displacement curve. Note that for the load displacement relationships that are the same for both positive and negative displacement (which is the case for nail connections), the absolute values of both P_1 , and P_2 , for both negative and positive force will be the same. A typical loading path is shown in Fig. 5(b). The parameter α , as previously mentioned, controls the unloading stiffness. If an empirically determined unloading stiffness K_3 is used (for unloading originating at the (F_{ult}, δ_{ult}) coordinate), the parameters α and β are determined in reference to Fig. 5(c).

From Fig. 5(c), α is found by

$$\alpha = \frac{K_3 \delta_{ult} - F_{ult}}{F_y - K_3 \delta_y} \quad (8)$$

β is simply the ratio of F_1 (pinching strength) to F_y

$$\beta = \frac{F_1}{F_y}, \quad 0 < F_1 \leq F_y \quad (9)$$

The entire process to produce the force-displacement relationship for a nail is summarised using the following example for 3 mm diameter nails connecting 11 mm OSB sheathing to spruce-pine-fir (SPF) framing (nails in single shear). Note that the same relationship is applied to both the U_2 and U_3 directions.

Step 1

Consider specific gravities of sheathing and framing. From Table 2, SG (OSB) = 0.64, and SG (SPF) = 0.42.

Step 2

Use the EYM theory to calculate the theoretical lateral strength $F_{ult(EYM)}$. Using the formulas provided by the American Forest and Paper Association (1999), the value of 928 N is calculated for this example. These calculations were also used to produce the graphs of Figs. 3(a) and 3(b). For this example of a nail in single shear, the value of $F_{ult(EYM)} = 928$ N can be obtained also from Fig. 3(a).

Step 3

Adjust $F_{ult(EYM)}$ to provide the actual F_{ult} value (hereafter referred to simply as F_{ult}). Eq. (4) (for single-shear) is used. The calculated value of F_{ult} is found to be 1256 N.

Step 4

Adjust the benchmark force-displacement relationship of Section 2.1 to reflect the calculated F_{ult} (1256 N) of Step 3. F_{ult} for the benchmark force-displacement curve is 1370 N (see Table 1). Thus the force-displacement envelope curve for the particular nail connection of this example is obtained simply by multiplying each of the force values of the reference curve by 1256 N/1370 N (0.92). The resulting load displacement curve is shown in Fig. 6.

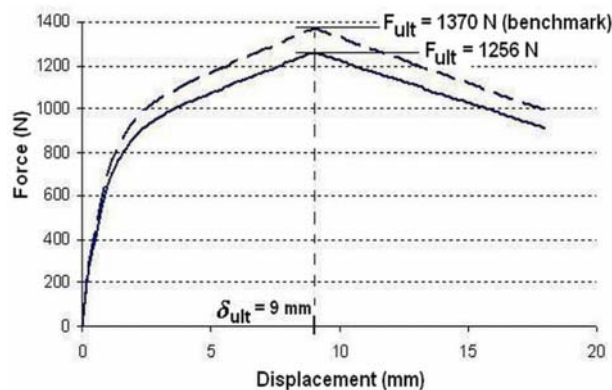


Fig. 6 Force-displacement envelope for $F_{ult} = 1256$ N (solid line), compared with benchmark curve of $F_{ult} = 1370$ N (broken line)

Note that the pinching strength originally determined by Dolan and Madsen (1992) of $F_1 = 193$ N (see Table 1) is adjusted using the same ratio of 0.92. Hence, the modified pinching strength is now $0.92 \times 193 = 177.6$ N.

Step 5

Using the point terminating the first linear segment of the defined force-displacement curve, (δ_y, F_y) , determine the hysteresis parameters α and β .

Note that (δ_y, F_y) has no particular significance, aside from being the end-point of the first linear segment used to define the force-displacement envelope. However, care must be taken to choose (δ_y, F_y) so that F_y is greater than or equal to the pinching strength, F_1 , because β is required to be less than or equal to 1 (see Eq. (9)). The first segment on the force-displacement envelope for this example is defined as a line between the origin and the point $(\delta_y, F_y) = (0.00018 \text{ m}, 195.5 \text{ N})$. A K_3 value of 674,000 N/m is adopted according to results of experiments performed by Blassetti *et al.* (2008). By inputting $\delta_{ult} = 0.009 \text{ m}$, $F_{ult} = 1256 \text{ N}$, $F_y = 195.5 \text{ N}$, $\delta_y = 0.00018 \text{ m}$, and $K_3 = 674,000 \text{ N/m}$ into Eq. (8), a value of 64.8 is obtained for α . Parameter β which relates to the pinching strength is obtained from Eq. (9), i.e., $\beta = 177.6/195.5 = 0.91$

Step 6

Define a new multi-linear plastic link element and input the force-displacement relationship, and associated hysteretic parameters. This is carried out for the two shear directions U_2 , and U_3 . The remaining four degrees of freedom are left unrestrained.

Verification of model nail

To verify the nail model, an actual test result obtained by Blassetti *et al.* (2008) is used. The time-displacement protocol used is the CUREE displacement protocol recommended for the cyclic testing of nail connections (Fonseca *et al.* 2002). This displacement protocol consists of a series of displacement cycles, the amplitude of each cycle being a pre-defined multiple of a pre-selected reference displacement. For the considered model nail the reference displacement of 4.3 mm used by Blassetti *et al.* (2008) for experimental testing, is adopted.

The hysteretic response of the model nail is compared with the experimental result reported by Dinehart *et al.* (2006) (see Fig. 7).

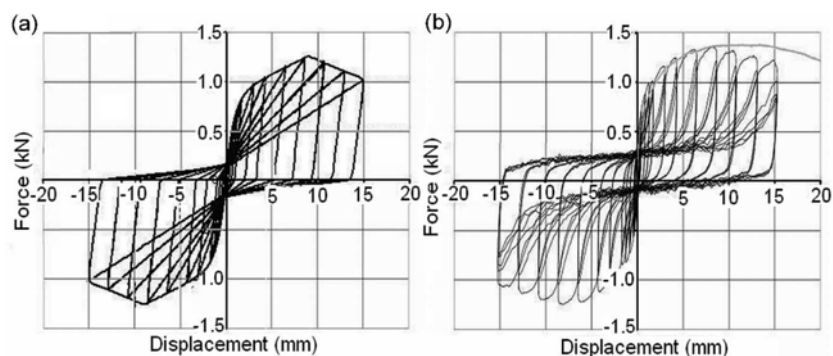


Fig. 7 Force-displacement relationship for 3 mm nails attaching 11 mm thick OSB sheathing to SPF framing (a) Numerical simulation and (b) experimental result (courtesy of Dinehart *et al.* (2006))

It can be seen that the response of the model nail provides a reasonably close representation to the response of the same nail under experimental loading.

3. Numerical simulation of shear wall behaviour

3.1 Modelling the walls

If non-linear behaviour is concentrated at the sheathing to framing nail connections, then the framing and sheathing elements can be assumed to be entirely elastic. This will save computational time. Nail elements are modelled using the procedure described in Section 2, and these elements are then used to attach framing to sheathing.

Beam elements (called frame elements in SAP2000) which model straight structural members connecting two points, and which include the effects of biaxial bending, torsion, axial deformation, and biaxial shear deformations along their respective lengths, are used to model the timber studs and bottom plate and top plates. These beam elements representing the timber framing are connected to one another by pin connections. Sheathing (shaded areas in Figs. 8(a), (b)) is modelled using shell elements, with only membrane actions considered. Nail elements attach the sheathing to framing; their locations are coincident with nodes on the meshed sheathing. The numerical model is verified using data obtained from experiments by other researchers.

It should be noted that the model walls, when loaded, are limited to displacements in the horizontal direction along the plane of the wall, and in the vertical direction. Thus the model restrains against out-of-plane displacements. However it is expected that any out-of-plane effects would likely have little influence on the overall force-displacement behaviour of the shear walls. This is because timber shear wall behaviour is largely governed by the hysteretic behaviour of the nail connections (Judd and Fonseca 2005).

3.2 Monotonic loading

The model walls with the method of load application are shown in Fig. 8.

For the standard wall (see Fig. 8(a)) the load is applied at the top of the wall via a very stiff linear spring (20 kN/mm), a roller joint, and a short metal rod. The load is thus resisted by both the wall

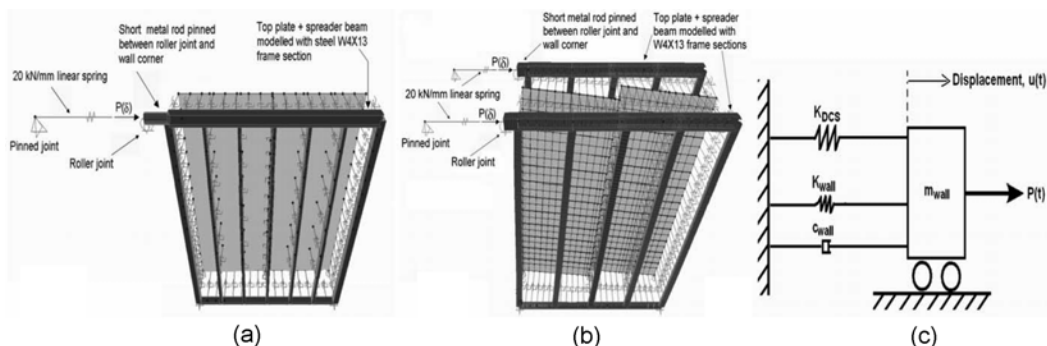


Fig. 8 Model walls with load application. (a) standard wall, (b) midply wall and (c) conceptualization of wall-displacement control spring

and the very stiff linear spring during loading. The racking force $F(\delta)$ is found by simply subtracting the force in the 20 kN/mm linear spring from $P(\delta)$.

$$F(\delta) = P(\delta) - K_{StiffSpring}\delta \quad (10)$$

If we assume a maximum displacement of 150 mm to be sufficient for simulation, the final applied force will be 20 kN/mm \times 150 mm = 3000 kN. The very stiff linear spring is provided to circumvent numerical convergence issues which would arise if only the wall itself was loaded, and displaced farther than the ultimate displacement, δ_{ult} , at which the peak load, F_{ult} , occurs. By adding the very stiff linear spring to the setup, the stiffness of the wall is essentially placed in parallel with the stiffness of the linear spring. $P(\delta)$ will then increase continuously during loading for all values of displacement, δ , and the numerical convergence problem is thus avoided. Racking force $F(\delta)$ on the wall at each displacement value is then obtained from Eq. (10).

For loading of the midply walls, two load applications are used (see Fig. 8(b)). A force $P(\delta=150 \text{ mm}) = 3000 \text{ kN}$ is applied at each load location. The stiffness of each of the two springs remains at 20 kN/mm, and the lateral force on the midply wall is given by Eq. (11).

$$F(\delta) = 2P(\delta) - 2K_{StiffSpring}\delta \quad (11)$$

3.3 Cyclic loading

The cyclic displacement load protocol adopted here for numerical simulation is based on the ISO 97 protocol used and described by Varoglu *et al.* (2006) in their testing of experimental shear walls. A typical ISO 97 displacement time-history schedule is shown in Fig. 12 of Section 4.2.

For the numerical simulation of dynamic loading a force time-history, $P(t)$, is specified and applied to the combined linear stiff spring and wall model as shown in Figs. 8(a), (b). A very stiff spring is used to control displacement, in a way similar to that adopted for monotonic testing.

This displacement control spring (hereafter referred to as the DCS) is pinned between a roller joint and pin joint to maintain a horizontal alignment. The total force $P(t)$ is applied at the roller joint. A short metal rod transfers lateral force to the top corner of the wall. Because the metal rod is pinned between the roller joint and the corner of the wall, there is no moment transfer between the force actuator and the wall.

The DCS is a linear spring - the force in the spring will increase indefinitely and linearly with increasing displacement. Hence, the DCS-shear wall system can be solved without a post ultimate-load numerical convergence issue occurring. The DCS-wall system can be conceptualised approximately as a mass/spring/damper system (Fig. 8(c)). Note that the stiffness of the spring representing the wall stiffness, K_{wall} , is nonlinear and varies with time during the displacement time-history loading.

The equation of motion is obtained by

$$P(t) = m_{wall}\ddot{u}(t) + c\dot{u}(t) + (K_{DCS} + K_{wall})u(t) \quad (12)$$

The wall mass, m_{wall} , is displaced at a constant rate in both directions. Hence, for each direction of loading the acceleration is zero and the activated inertial force $m_{wall}\ddot{u}(t) = 0$. Because the velocity \dot{u} is low, and the viscous damping ratio of 1%, recommended by Ayoub (2007), Xu and Dolan

(2009b) for the modelling of wood structures, is also low, $c\dot{u}$ is very small compared with $(K_{DCS} + K_{wall})u(t)$. Thus Eq. (12) reduces to Eq. (13)

$$P(t) \approx K_{DCS}u(t) + K_{wall}u(t) \quad (13)$$

Because K_{DCS} is very large relative to K_{wall} , the $(K_{wall}u(t))$ part of Eq. (11) can also be omitted. Eq. (13) thus reduces to Eq. (14)

$$P(t) \approx K_{DCS}u(t) \quad (14)$$

In this way, a force time-history function $P(t)$ can be constructed from a displacement time-history schedule $u(t)$. Note that $u(t)$ is the displacement time-history schedule applied at the top corner of the wall.

Upon completion of a load cycle, force $F(t)$ applied to the wall is determined at each time step by Eq. (15), which simply subtracts the force in the displacement control spring/s from the total horizontal force applied to the system.

$$F(t) = P(t) - K_{DCS}u(t) = m_{wall}\ddot{u}(t) + c\dot{u}(t) + K_{wall}u(t) \quad (15)$$

$F(t)$ also equates to the equation of motion of the model wall itself (without the displacement control spring). $F(t)$ is plotted against displacement to produce hysteresis loops for the considered model walls (see Fig. 13).

4. Verification of model walls

The results of monotonic and cyclic loadings on a range of numerically modelled shear walls, both standard and midply, are compared against results obtained from the experimental testing of actual shear walls.

4.1 Monotonic loading

Varoglu *et al.* (2006) reported on monotonic loading experiments carried out on a series of 2.4 m × 2.4 m standard walls and midply walls. Properties used to model framing lumber, and sheathing were sourced from the Canadian Wood Council (2009), and the Canadian Plywood Association (2009) respectively.

Seven of these walls - two standard walls, S31 and S37, and five midply walls, M25, M26, M27, M32 and M41, were modelled in this study. The walls all utilised framing members of 38 × 89 mm SPF. SPF was modelled using an MOE of 9500 MPa, and a density of 420 kg/m³. The stud spacing used for the standard walls was 406 mm. For midply wall M32, studs were spaced at 406 mm. The remaining midply walls had studs spaced at 610 mm.

For the standard walls, nails were spaced at 152 mm throughout and sheathing was of 9.5 mm thick CSP (density of 450 kg/m³, MOE of 5200 MPa, and shear modulus of 430 GPa). Wall S31 was placed under a distributed load (18.2 kN/m) acting down on its top plate, while wall S37 did not undergo any vertical loading. Walls M25, M26 and M27 utilised sheathing of 12.5 mm CSP

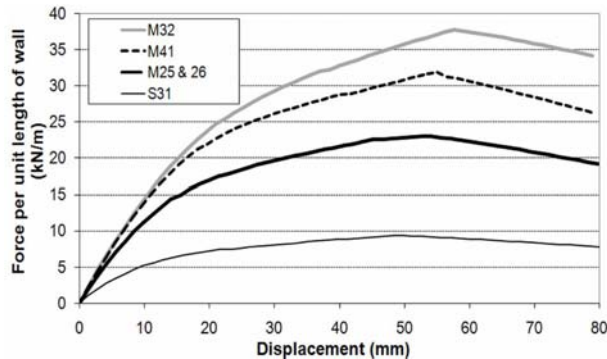


Fig. 9 Numerically determined force-displacement curves from monotonic load simulation

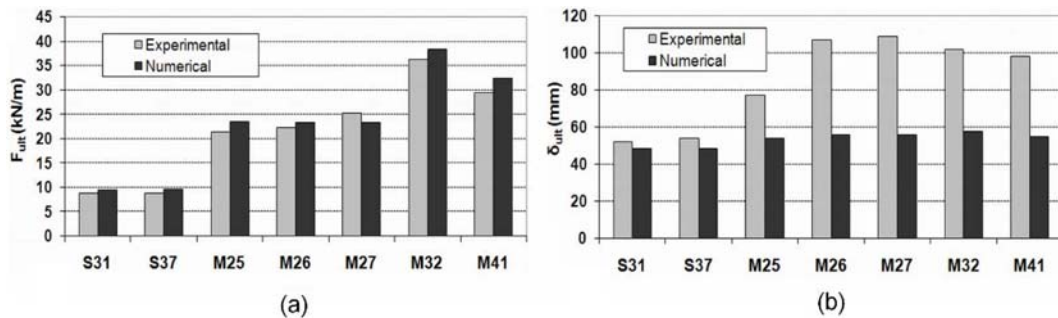


Fig. 10 Comparison of results for monotonic load case. (a) Ultimate strength, F_{ult} and (b) ultimate displacement, δ_{ult}

(density 450 kg/m^3 , MOE of 4940 MPa in its strong direction, and shear modulus of 430 GPa) with nail connections at 100 mm centre to centre. Walls M25 and M27 were placed under an 18.2 kN/m distributed load, while M26 incurred zero vertical loading.

Sheathing for walls M32 and M41 were of 12.5 mm OSB and 10.5 mm OSB respectively. A density of 640 kg/m^3 was used for OSB. For 12.5 mm OSB, an MOE of 3440 MPa and a shear modulus of 880 GPa was used. For 10.5 mm OSB, according to the Canadian Plywood Association (2009), both the MOE and shear modulus are slightly higher, with an MOE of 3460 MPa and a shear modulus of 984 GPa being used. Nails connecting sheathing to framing for walls M32 and M41 were spaced at 100 mm . Each of these two walls was placed under a distributed vertical load of 18.2 kN/m .

The nail connection force-displacement relationships were determined in accordance with Section 2. These nail connections were then incorporated into the model walls. The model walls were then monotonically loaded in the manner described in Section 3.1. The resulting force-displacement curves are shown in Fig. 9.

For the ultimate lateral strength, F_{ult} , there is excellent agreement between numerical and experimental results (Fig. 10(a)). For displacement at peak load, δ_{ult} , (Fig. 10(b)) there is excellent agreement between the numerical and experimental results for the two standard walls, but not for the midply walls. For the midply walls, the numerical analyses all significantly underestimate the experimental results.

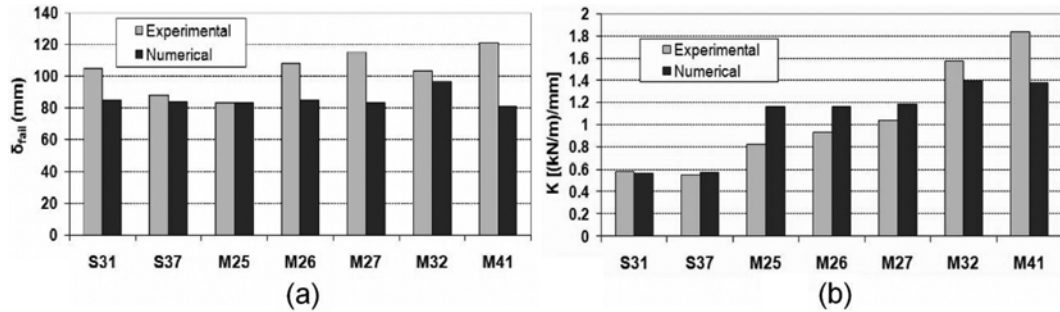


Fig. 11 Comparison of results for monotonic load case (a) failure displacement, δ_{fail} , and (b) secant stiffness, K , numerical vs. experimental

The discrepancies can possibly be accounted for by the damage to framing and sheathing observed in the experimental midply walls during loading. It is unlikely that these large discrepancies are related to the uncoupled nail model adopted, as results from researchers, such as Judd and Fonseca (2005), show that the difference between ultimate displacements for model walls with uncoupled nail models, and actual experimental walls is actually quite small. For walls M26, M27, and M41, slippages of the top plate relative to the top of studs were recorded. Wall M26 also had nails withdrawing along the joint stud, while wall M32 showed some local fracture in the OSB panel near one of its hold-down connectors (Varoglu *et al.* 2006).

Note that the occurrence of nail withdrawals and plate slippage, and even fracturing of sheathing would not necessarily lead to an immediate loss in strength, but rather a loss of stiffness, thereby increasing the displacement at which the ultimate load is finally achieved.

Because the proposed modelling approach only considers nonlinearities at the sheathing-to-framing nail connections, the effect of nonlinear damage to framing or sheathing would not have been detected by the model walls.

For failure displacement, δ_{fail} , (see Fig. 11(a)) very good agreement between numerical and experimental results is obtained for walls S31, S37, and M25. Note that failure displacement δ_{fail} is the displacement at which the strength of the wall first descends to 80% of F_{ult} , after F_{ult} has already been achieved.

Because of limitations of the load actuator used in the experimental setup, the failure displacements for midply walls M26, M27, M32, and M41 in Fig. 11(a) are minimum possible values only. It can be seen that even these minimum values already exceed those provided by the numerical model. However, this is to be expected, as ultimate displacements for the experimental midply walls (see Fig. 10(b)) also exceed those of their numerical counterparts - for reasons already discussed.

The wall stiffness, K , is commonly defined in terms of secant stiffness per metre length of wall. Varoglu *et al.* (2006) determined K as follows

$$K = 0.3F_{ult}/[(\delta_{0.4F_{ult}} - \delta_{0.1F_{ult}})L] \quad (16)$$

From Fig. 11(b) it can be seen that for secant stiffness, K , there is excellent agreement between experimental and numerical results for the standard walls and reasonably good agreement for the midply walls.

4.2 Cyclic loading

In addition to the monotonic tests described in Section 4.1, Varoglu *et al.* (2006) carried out cyclic tests on a series of shear walls. Force-displacement data for three of these walls (midply walls M29, M30, and M31) were made available, courtesy of Dr M. Popovski of FPInnovations in Canada. Also provided was force-displacement data for two standard walls designated 30-04 and 48-28. Note that these two standard walls were not part of the group of walls tested and described by Varoglu *et al.* (2006).

These five walls were numerically modelled and analysed under cyclic loading. The numerical loading mirrored that of the actual experimental conditions of testing for both the standard and midply walls. The force-displacement results of the model walls are compared with the experimentally obtained results to verify the adequacy of the numerical model.

All walls were 2.44 m high. Apart from wall 30-04 (4.8 m long), walls were all 2.44 m long. Sheathing for all walls was CSP, 9.5 mm thick for the standard walls, and 12.5 mm thick for the midply walls. Studs were modelled as SPF. Material properties for SPF studs and CSP sheathing were the same as those used in Section 4.1. Studs were spaced at 406 mm for the two standard walls and 610 mm for the midply walls. Nail diameters were all 3 mm. For both standard walls and also midply wall M29, nails were spaced at 150 mm. For M30 and M31 nails were spaced at 100 mm. The force-displacement relationships for the nail connections were determined in accordance with the procedure detailed in Section 2.3. For enhanced computational efficiency, one nail element was used to lump together four actual nails. Quick monotonic loadings were carried out on the same wall configuration, with and without lumping of nails, to confirm the force-displacement envelopes obtained from these loadings matched each other, and hence verified the validity of lumping the nails.

Walls 30-04 and M31 were not subject to vertical loading. Walls 48-28, M29, and M30 were each subjected to an 18.2 kN/m vertical distributed load at the top of wall. For actual experimental testing, a spreader beam was rigidly attached to the top plate, and the bottom plate rigidly bolted to the base of the test rig. Thus, the top and bottom plates were modelled by SPF framing lumber (same as for studs) but with the MOE multiplied by a factor of 100, in order to minimise bending deformations.

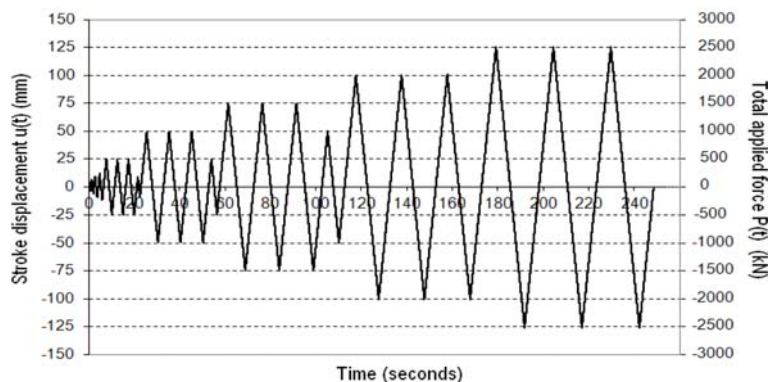


Fig. 12 Displacement time-history, $u(t)$, used in the experiments and force schedule, $P(t)$, for wall M30 applied in the numerical simulation (for one displacement control spring)

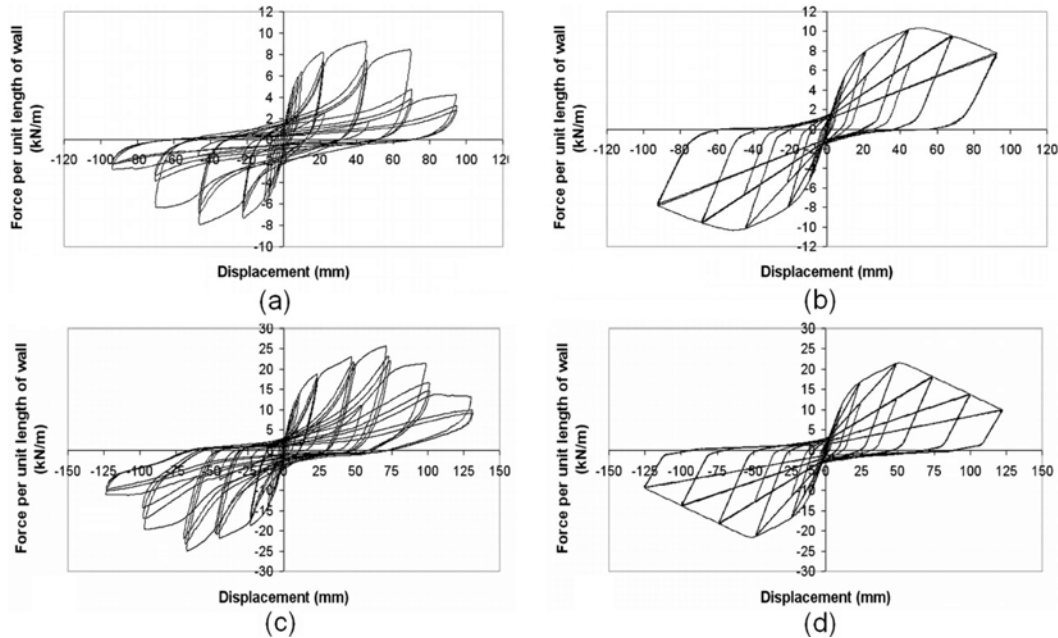


Fig. 13 Hysteretic response of walls: Standard wall 48-28, (a) experimental, vs. (b) numerical response; and midply wall M29, (c) experimental, vs. (d) numerical response

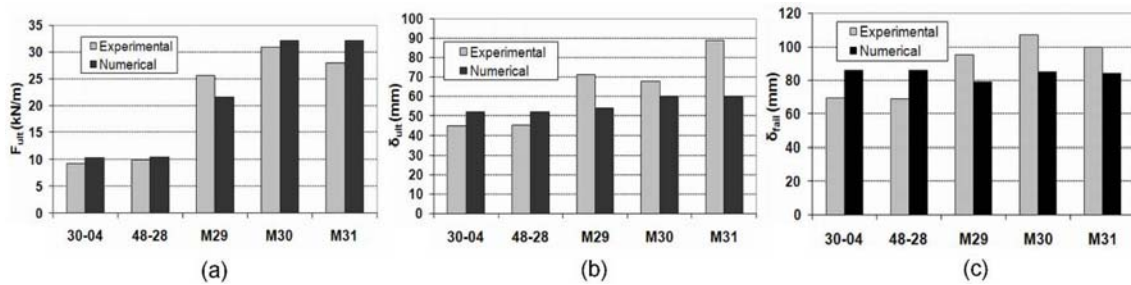


Fig. 14 Cyclic load cases, numerical vs. experimental: (a) ultimate lateral strength, F_{ult} , (b) ultimate displacement, δ_{ult} and (c) failure displacement, δ_{fail}

From the force-displacement data provided, the displacement time-history schedule was determined for each wall. For each wall, Eq. (14) was used to convert the displacement time-history schedule to a force time-history schedule for determination of loading for the numerical simulation, $P(t)$. The displacement control springs for both standard walls and midply walls had an assigned stiffness of $K_{DCS} = 20 \text{ kN/mm}$ (two springs, one for each framing layer in the case of midply walls). The displacement time-history schedule, $u(t)$, and corresponding force time-history schedule, $P(t)$, are displayed on the same chart. Fig. 12 shows this for wall M30.

The Wilson fast-nonlinear-analysis (FNA) method was used for the analysis. A time step of 0.01 seconds was chosen. Viscous damping was set to 1% for all modes of vibration. The relevant force time-history function $P(t)$ was applied to the walls. On completion of each load cyclic, $F(t)$ for each wall was calculated from Eq. (15). $F(t)$ was then plotted against $u(t)$ in order to obtain the

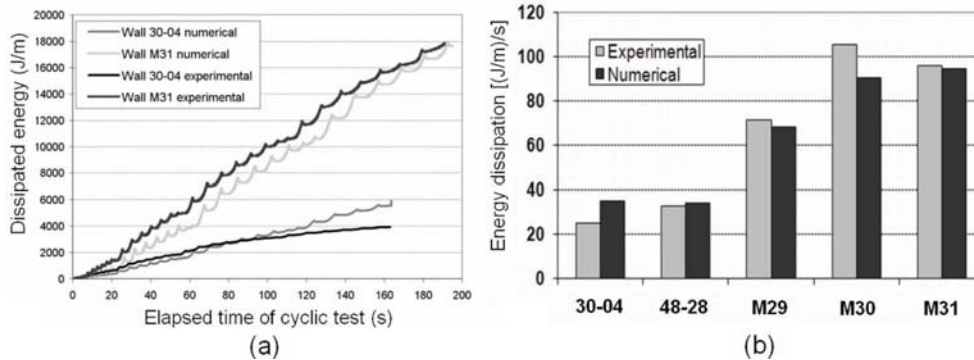


Fig. 15 Numerical vs. experimental: (a) energy dissipation for wall 30-04 & M31, (b) energy dissipation rates

corresponding force-displacement relationships.

The numerical results for all five walls compared well with the response of their experimental counterparts. Fig. 13 shows the experimental and numerical results for two of these walls; standard wall 48-28, and midply wall M29.

For the ultimate lateral strength, F_{ult} , the numerical results show good agreement with the experimental (see Fig. 14(a)).

Fig. 14(b) shows excellent agreement between numerical and experimental values for the ultimate displacement, δ_{ult} , for standard walls 30-04 and 48-28, and reasonable agreement for the midply walls (except for M31).

For wall M31, the displacement δ_{ult} for the model wall is only 67% of the value obtained experimentally. However, for the M31 experimental wall, it was reported by Varoglu *et al.* (2006) that the top plate separated from the top end stud near the actuator. As the walls were numerically modelled with the studs pinned securely to the top plates, it is concluded that the discrepancy between numerical and experimental can be explained by this slippage of the top plate during actual experimental testing.

Fig. 14(c) shows values for the *failure displacement*, δ_{fail} . It can be seen that there is reasonably good agreement between numerical and experimental values for δ_{fail} for all of these walls.

Figs. 15(a) compares the numerically and experimentally observed energy dissipation, for standard wall 30-04, and midply wall M31. Fig. 15(b) compares the rate of energy dissipation for all five model walls with the experimental results.

Of the five walls, it can be seen that wall 30-04 is the only wall in which the numerical result shows significant discrepancy from the experimental results (Fig. 15(b)). From the force-displacement record of wall 30-04 (not presented here) there was a sudden and precipitous loss in strength, beyond the ultimate displacement (compared to the record for the other walls). This sudden decline in strength of wall 30-04 likely indicates that nonlinear failure of the framing or sheathing material occurred. This nonlinear failure would not have been identified by the numerical model, in which nonlinearities are modelled only at the sheathing-to-framing nail connections.

For the other walls, it is clear from Fig. 15(b) that the model walls closely replicate the energy dissipation characteristics of the experimental walls.

5. Conclusions

A numerical approach to simulate the behaviour of timber shear walls under monotonic and cyclic loading is proposed. Because the force-displacement behaviour of the nails governs overall shear wall behaviour, the nail connections are carefully modelled using the well-established Foschi exponential curve, with this curve being adjusted to account for differences in connection strengths. The connection strengths are arrived at by using a mechanics based analytical approach. A relationship is found between these theoretical values of connection strength and values obtained from experimental testing. This is done for both the single shear nail connections used in standard shear walls, and the double shear nail connections used in midply walls.

The approach proposed is verified using experimental results. Under monotonic and cyclic loading, the model walls (both standard and midply) have been found to provide a good representation of actual shear wall behaviour. Where significant discrepancies were observed between numerical and experimental results, it was found that these could be mainly attributed to nonlinear damage to framing and/or sheathing which occurred during experimental testing, since the model walls consider nonlinear behaviour at the nail connections only.

Damage such as cracking of sheathing, slippage of top plates, and buckling of studs, are not implemented in the numerical model. However, this should not compromise the effectiveness of the proposed approach, because stresses at any location in a model wall during loading can be readily tracked and analysed. From the stress levels observed, it can be seen whether or not the elastic limits of the framing and sheathing would have been exceeded. Hence a reasonable expectation of the likelihood of damage occurring can be obtained.

The proposed numerical method for the modelling of timber shear walls has the potential to offer researchers and practicing engineers a quick and reliable means of investigating and observing the influence of different loading regimes on the force-displacement response of timber shear walls of various structural configurations.

Acknowledgements

The authors would like to express their appreciation to the New Zealand Ministry of Agriculture and Forestry for supporting this research, and the anonymous reviewers for their constructive comments that have improved the clarity of this article.

References

- Aghayere, A. and Vigil, J. (2007), *Structural Wood Design: A Practice-oriented Approach Using the ASD Method*, John Wiley and Sons Inc., New York.
- American Forest and Paper Association (1999), *General Dowel Equations for Calculating Lateral Connection Values*, Technical Report 12, Washington D. C.
- Ayoub, A. (2007), "Seismic analysis of wood building structures", *Eng. Struct.*, **27**(2), 213-223.
- Blasetti, A.S., Hoffman, R. and Dinehart, D. (2008), "Simplified hysteresis finite-element model for wood and viscoelastic polymer connections for the dynamic analysis of shear walls", *J. Struct. Eng.*, **134**(1), 77-86.
- Buchanan, A. (2007), *Timber Design Guide*, 3rd Editions, Timber Industry Federation Inc, Wellington, New Zealand.

- Canadian Plywood Association (2009), "Comparative engineering properties: Plywood and OSB", http://www.canply.org/english/products/comparison/comparison_all.htm. (accessed Jan 12, 2009)
- Canadian Wood Council (2009), "Lumber", <http://www.cwc.ca/products/lumber>. (accessed Jan 12, 2009)
- CertiWood (2004), *Plywood design fundamentals*, CertiWood Technical Centre, Canada.
- Computers and Structures, Inc. (2009), *SAP2000 v14: Integrated Solution for Structural Analysis and Design*, Berkeley, California.
- Coyne, T. (2007), "NEES Wood: Framing to sheathing connection tests", *Proceedings of Earthquake Engineering Symposium for Young Researchers*, University at Buffalo, Seattle, August.
- Dinehart, D.W., Hoffman, R.M. and Blasetti, A.S. (2006), "Finite element modeling of wood shear walls with viscoelastic polymers", *Proceedings of the 9th World Conference on Timber Engineering*, Oregon, August, Portland.
- Dolan, J.D. and Madsen, B. (1992), "Monotonic and cyclic nail connection tests", *Can. J. Civil*, **19**(1), 97-104.
- Ekiert, C. and Hong, J. (2006), *Framing-to-sheathing Connection Tests in Support of NEES Wood Project: Technical Report*, University at Buffalo, NY.
- Fonseca, F.S., Judd, J.P. and Burns, J.M. (2006), "Strength of plywood joints with overdriven nails", *Forest Prod J.*, **56**(7/8), 33-38.
- Fonseca, F.S. and Rabe, J.A. (2009), "Capacity of oriented strandboard joints with overdriven nails", *Forest Prod J.*, **59**(4), 50-60.
- Fonseca, F.S., Rose, S.K. and Campbell, S.H. (2002), *CUREE Publication No. W-16: Nail, Wood Screw, and Staple Fastener Connections*, Richmond, Calif.
- Judd, J.P. and Fonseca, F.S. (2005), "Analytical model for sheathing-to-framing connections in wood shear walls and diaphragms", *J. Struct. Eng.*, **131**(2), 345-352.
- NZS3603 (1993), *Timber Structures Standard*, Standards New Zealand, Wellington, New Zealand.
- Smith, I., Craft, S.T. and Quenneville, P. (2001), "Design capacities of joints with laterally loaded nails", *Can. J. Civil*, **28**(2), 282-290.
- Structural Board Association (2004), *OSB Performance by Design: Oriented Strand Board in Wood Frame Construction*, Canada.
- Thelandersson, S. and Larsen, H. (2003), *Timber Engineering*, John Wiley and Sons Ltd., West Sussex, England.
- U.S. Department of Agriculture (2010), *Wood Handbook: Wood as an Engineering Material*, Forest Products Laboratory, Madison, Wisconsin.
- Varoglu, E., Karacabeyli, E., Stiemer, S. and Ni, C. (2006), "Midply wood shear wall system: Concept and performance in static and cyclic testing", *J. Struct. Eng.*, **132**(9), 1417-1425.
- Vessby, J., Serrano, E. and Olsson, A. (2010), "Coupled and uncoupled nonlinear elastic finite element models for monotonically loaded sheathing-to-framing joints in timber based shear walls", *Eng. Struct.*, **32**(11), 3433-3442.
- Xu, J. and Dolan, J.D. (2009a), "Development of nailed wood joint element in ABAQUS", *J. Struct. Eng.*, **135**(8), 968-976.
- Xu, J. and Dolan, J.D. (2009b), "Development of a wood-frame shear wall model in ABAQUS", *J. Struct. Eng.*, **135**(8), 977-984.

Notations

The following symbols are used in this paper:

c	= viscous damping coefficient
CSP	= Canadian softwood plywood
D	= nail diameter
DCS	= displacement control spring
EYM	= European yield model
F_0	= intercept of secondary stiffness line of a nail connection with the y (force) axis
F	= racking force on wall
F_1	= pinching strength of a nail connection
$F_{b,ult}$	= dowel bending strength of a nail connection
F_{uef}	= Ultimate strength of double-shear nail connection including end-fixity effects
$F_{e,ult}$	= dowel bearing strength of a nail connection
F_{ult}	= ultimate lateral strength of a nail connection or shear wall
$F_{ult(EYM)}$	= ultimate lateral strength of a nail connection as determined by EYM theory
F_y	= yield strength of a nail connection
G	= shear modulus
K	= stiffness of shear wall
K_0	= initial stiffness of a nail connection
K_1	= secondary stiffness of a nail connection
K_2	= degrading stiffness of a nail connection
K_3	= unloading stiffness of a nail connection
L	= length of wall
m	= mass
MOE	= modulus of elasticity
OSB	= oriented strand board
P	= Total lateral force applied to a wall system including displacement control spring
SG	= specific gravity
SPF	= Spruce pine fir (Canadian)
t	= time elapsed during cyclic test
u	= displacement
\dot{u}	= velocity
\ddot{u}	= acceleration
U_1	= translation along local axis 1 of link element
U_2	= translation along local axis 2 of link element
U_3	= translation along local axis 3 of link element
α	= parameter used to define unloading stiffness of finite element representation of nail connection
β	= parameter used to define the unloading stiffness of finite element representation of nail connection
δ	= lateral displacement of a shear wall or nail connection
δ_{fail}	= Displacement of shear wall corresponding to $0.8F_{ult}$, on the degrading portion of the force-displacement curve
δ_{ult}	= displacement corresponding to the ultimate lateral strength of a shear wall or nail connection
δ_y	= yield displacement of a nail connection
$\delta_{0.1F_{ult}}$	= displacement at $0.1F_{ult}$ on the ascending portion of a force-displacement curve
$\delta_{0.4F_{ult}}$	= displacement at $0.4F_{ult}$ on the ascending portion of a force-displacement curve